Observations of OH and HO2 radicals in coastal Antarctica

W. J. Bloss, J. D. Lee, D. E. Heard, R. A. Salmon, S. J.-B. Bauguitte, H. K. Roscoe, A. E. Jones

Atmos. Chem. Phys., 7, 4171–4185, 2007
www.atmos-chem-phys.net/7/4171/2007/

Atmospheric Chemistry and Physics

Observations of OH and HO_2 radicals in coastal Antarctica

W. J. Bloss[1,*], J. D. Lee[1,], D. E. Heard[1], R. A. Salmon[2], S. J.-B. Bauguitte[2], H. K. Roscoe[2], and A. E. Jones[2]**

[1]School of Chemistry, University of Leeds, Woodhouse Lane, Leeds, LS2 9JT, UK
[2]British Antarctic Survey, Madingley Road, Cambridge, CB3 0ET, UK
[*]now at: School of Geography, Earth & Environmental Sciences, University of Birmingham, Edgbaston, Birmingham, B15 2TT, UK
[**]now at: Department of Chemistry, University of York, Heslington, York, YO10 5DD, UK

Received: 18 January 2007 – Published in Atmos. Chem. Phys. Discuss.: 23 February 2007
Revised: 27 July 2007 – Accepted: 10 August 2007 – Published: 16 August 2007

Abstract. OH and HO_2 radical concentrations have been measured in the boundary layer of coastal Antarctica for a six-week period during the austral summer of 2005. The measurements were performed at the British Antarctic Survey's Halley Research Station (75° 35′ S, 26° 19′ W), using the technique of on-resonance laser-induced fluorescence to detect OH, with HO_2 measured following chemical conversion through addition of NO. The mean radical levels were 3.9×10^5 molecule cm^{-3} for OH, and 0.76 ppt for HO_2 (ppt denotes parts per trillion, by volume). Typical maximum (local noontime) levels were 7.9×10^5 molecule cm^{-3} and 1.50 ppt for OH and HO_2 respectively. The main sources of HO_x were photolysis of O_3 and HCHO, with potentially important but uncertain contributions from HONO and higher aldehydes. Of the measured OH sinks, reaction with CO and CH_4 dominated, however comparison of the observed OH concentrations with those calculated via the steady state approximation indicated that additional co-reactants were likely to have been present. Elevated levels of NO_x resulting from snowpack photochemistry contributed to HO_x cycling and enhanced levels of OH, however the halogen oxides IO and BrO dominated the CH_3O_2 – HO_2 – OH conversion in this environment, with associated ozone destruction.

1 Introduction

The chemistry of the sunlit troposphere is dominated by the reactions of the hydroxyl radical, OH, which is responsible for initiating the degradation of most hydrocarbons and other species emitted to the atmosphere. Knowledge of atmospheric hydroxyl levels, of related species such as HO_2, and the chemical processes which govern their abundance, is central to explaining current atmospheric trace gas distributions and predicting their likely future evolution.

Correspondence to: W. J. Bloss
(w.j.bloss@bham.ac.uk)

Field measurement campaigns, in which coordinated measurements of radical species such as OH, HO_2, NO etc. have been performed, provide a means to test and refine our understanding of fast radical photochemistry. Measurements of OH and HO_2 radicals have been performed in a range of marine and continental, polluted and clean environments (e.g. Heard and Pilling, 2003, and references therein); however very few measurements have been performed in the polar boundary layer, where the differing physical conditions together with snowpack emission and deposition processes give rise to a unique chemical environment.

Interest in the chemistry of the polar boundary layer, and the atmospheric chemistry above the surface of the polar ice sheets and sea ice, has grown in recent years, driven in part by interest in understanding atmospheric evolution through measurements of trace gases in air trapped in ice cores and firn. In addition to climatic information derived from long-lived tracers such as CO_2 levels and various isotope ratios, measurements of sulphur, nitrate and peroxide levels have all been used to infer historic atmospheric composition (e.g. Legrand and Mayewski, 1997, and references therein); understanding the chemical environment in which these species are deposited and incorporated in firn/ice, i.e. the background chemistry of the polar boundary layers, is clearly important for such analyses.

From the perspective of the modern atmosphere, interest in the polar boundary layer has also been driven by the observation of periodic surface ozone depletion events linked to bromine chemistry in the arctic, and the recognition that snowpack can act as a source of nitrogen oxides NO and NO_2 (collectively NO_x), HONO, HCHO and peroxides, amongst other species, thereby modifying the boundary layer composition from what might be expected for regions remote from pollutant sources.

In the sunlit background troposphere, radical production is driven primarily by the short-wavelength photolysis of ozone, and reaction of the electronically excited $O(^1D)$ atoms

so formed with water vapour (in competition with quenching), forming hydroxyl radicals:

$$O_3 + h\nu \rightarrow O(^1D) + O_2 \quad \text{(R1)}$$

$$O(^1D) + H_2O \rightarrow OH + OH \quad \text{(R2)}$$

OH subsequently reacts with hydrocarbons such as methane, and with carbon monoxide, forming organic and hydroperoxy radicals respectively:

$$OH + CH_4(+O_2) \rightarrow CH_3O_2(+H_2O) \quad \text{(R3)}$$

$$OH + CO(+O_2) \rightarrow HO_2(+CO_2) \quad \text{(R4)}$$

The fate of the peroxy radicals depends upon the level of NO_x (=[NO] + [NO_2]). In clean (low NO_x) conditions, the peroxy radicals largely undergo self- or cross-reaction, leading to the formation of peroxides, alcohols and aldehydes, and in very low NO_x environments, ozone destruction results (via Reaction R1). Alternatively, peroxy radicals may react with NO, converting CH_3O_2 into HO_2 (and HCHO), and HO_2 into OH, with associated NO to NO_2 conversion:

$$CH_3O_2 + NO(+O_2) \rightarrow HCHO + NO_2 + HO_2 \quad \text{(R5)}$$

$$HO_2 + NO \rightarrow OH + NO_2 \quad \text{(R6)}$$

NO_2 in turn readily undergoes photolysis in the lower atmosphere leading to the formation of ozone.

$$NO_2 + h\nu \rightarrow NO + O \quad \text{(R7)}$$

$$O + O_2 + M \rightarrow O_3 + M \quad \text{(R8)}$$

The presence of NO_x thus leads to $RO_2 \rightarrow HO_2 \rightarrow OH$ radical cycling and to ozone production. Additional HO_x reservoir/sink formation also occurs, through the production of nitric acid and peroxynitric acid, and at sufficiently high levels of NO_x, removal of HO_x through HNO_3 formation leads to reduced ozone production.

$$OH + NO_2 + M \rightarrow HNO_3 + M \quad \text{(R9)}$$

$$HO_2 + NO_2 + M \leftrightarrow HO_2NO_2 + M \quad \text{(R10)}$$

In the polar boundary layers, solar insolation is low due to the high latitude (zero for significant periods of the year polewards of the Arctic/Antarctic circles) and water vapour concentrations are low (relative to lower latitudes) due to the low temperatures. Consequently, OH formation through Reactions (R1) and (R2) is slow, and in the absence of other factors HO_x levels are therefore expected to be low (the low concentrations of OH sinks, VOCs – volatile organic compounds – notwithstanding), with HO_x removal dominated by HO_2 radical recombination.

The first measurements of OH in Antarctica (Jefferson et al., 1998) were consistent with this picture, with mean 24-h OH levels of (1.1–16.1) $\times 10^5$ molecule cm^{-3} (typical maximum daily levels of $7\times$ 10^5 molecule cm^{-3}) reported during February at Palmer Station, a marine site on the Antarctic Peninsula (64.7° S). Subsequent studies in the Arctic and Antarctic identified snowpack as sources of several reactive species: HCHO (Sumner and Shepson, 1999; Hutterli et al., 1999), NO_x (Honrath et al., 1999; Jones et al., 2000), HONO (Zhou et al., 2001) and higher aldehydes (Grannas et al., 2002).

Such emissions will significantly alter the anticipated HO_x levels: HONO will readily undergo photolysis to release OH and NO, which together with potential direct NO_x emissions will drive radical cycling mechanisms, resulting in elevated HO_x, and potentially net ozone production.

$$HONO + h\nu \rightarrow OH + NO \quad \text{(R11)}$$

Measurements of OH performed at South Pole found much higher levels than those observed at Palmer Station; average values of (2–2.5) $\times 10^6$ cm^{-3} were reported during the austral summers of 1998 and 2000 (Mauldin et al., 1999, 2004). These levels can be compared with the daily maximum levels (7×10^5 cm^{-3}) from Palmer Station, considering the near-constant solar zenith angle at South Pole. The high levels of OH were consistent with rapid radical cycling (Reactions R5, R6) driven by snowpack emissions of NO_x, the effect of which was enhanced by the low boundary layer height at South Pole station (Chen et al., 2001; Davis et al., 2001). While agreement between observed and modelled OH and HO_2+ RO_2 levels was satisfactory for moderate levels of NO (ca. 100 ppt in this environment), at lower and higher NO levels the model over predicted the observed OH; moreover inclusion of measured HONO levels in the model led to a large overestimate of the measured OH and HO_2 + RO_2 levels (Chen et al., 2004). (ppt denotes parts per trillion, by volume).

Measurements of OH and HO_2+RO_2 have also been made at Summit, Greenland (at an altitude of 3200 m) during boreal summer 2003 and spring 2004. Noontime OH and peroxy radical levels of (5–20) $\times 10^6$ and (2–5) $\times 10^8$ cm^{-3} were observed (Huey et al., 2004; Sjostedt et al., 2005). Model calculations were able to reproduce the observed peroxy radical levels, but underestimated the OH concentrations, suggesting a missing HO_2 to OH conversion process, ascribed to possible bromine chemistry (Sjostedt et al., 2005).

A wide variation in radical concentrations is thus observed in overtly similar polar environments, probably driven largely by differences in local dynamical factors (stability/boundary layer height) and as a consequence of processes within the snowpack leading to the production of NO_x, HONO, aldehydes and halogen species amongst others. It was within this context that the CHABLIS campaign (Chemistry of the Antarctic Boundary Layer and the Interface with Snow) originated. CHABLIS aimed to make a series of measurements of atmospheric and firn air composition

in coastal Antarctica over a 13 month period from January 2004.

This paper describes measurements of OH and HO_2 radicals performed by laser-induced fluorescence (LIF) during the January and February 2005 CHABLIS oxidant intensive, at the British Antarctic Survey's Halley Research Station in coastal Antarctica. The measurement approach and calibration details are described, followed by a description of the data series, and correlations with radiation, meteorology and chemical composition. A steady-state analysis is used to qualitatively identify the likely dominant OH sources and sinks, and the data are discussed in relation to previous observations of HO_x in comparable locations. A separate paper (Bloss et al., 2007[1]) reports the results of a detailed photochemical modelling study of all the radical species observed, including a quantitative comparison of measured and modelled HO_2, overall radical sources/sinks and summarises the oxidative environment.

2 Measurement location/environment

Measurements were performed in the course of the CHABLIS campaign, a consortium project involving the British Antarctic Survey and the UK Universities of Leeds, York, East Anglia, Bristol and Imperial College. Full details of the project are given in the overview paper (Jones et al., 2007[2]) accompanying this special issue; brief details pertinent to the HO_x dataset are given here.

Measurements were made at the British Antarctic Survey's Halley Research Station, located on the Brunt Ice Shelf off Coats Land, at 75° 35′ S, 26° 19′ W. The base location is approximately 35 m above sea level. The base is located on a peninsula of the ice sheet, surrounded by the Weddell Sea to the North around (counter clockwise) to the South West, with the permanent ice front located 15–30 km from the base depending upon direction. The OH and HO_2 observations were made during the austral summer, January–February 2005, at which time the sea ice cover had almost entirely dissipated. The prevailing wind is from ca. 80 degrees, corresponding to a uniform fetch of several hundred km over the ice shelf. The measurement site was located ca. 1.5 km upwind of the other base buildings (and generators), at the apex of a clean air sector encompassing the prevailing wind direction, within and above which vehicle and air traffic movements were prohibited.

The LIF measurement system was located in a shipping container positioned 30 m from the Clean Air Sector laboratory (CASLab), which housed the remaining instrumentation. The container was mounted on a sledge, giving a sampling height for OH and HO_2 of approximately 5–4.5 m above the snow surface (range due to snow accumulation during the measurement period). Measurements of temperature, ambient humidity and ozone were co-located with the HO_x inlet. The light path of the DOAS instrument was at the same height, while the remaining species measured in ambient air (summarised below) were sampled from an inlet on the CASLab, approximately 8 m above the snow surface. The additional measurements referred to in this paper were NO/NO_2 (measured by chemiluminescent analyser with photolytic converter), O_3 (measured by UV absorption), H_2O (dew point hygrometer), CO (VUV fluorescence, calibrated by UK National Physical Laboratory standard), HCHO (fluorescence), non-methane hydrocarbons (NMHCs; detected by gas chromatography with flame ionisation detection (GC-FID) – Read et al., 2007), the halogen oxides IO and BrO (observed by differential optical absorption spectroscopy (DOAS) – Saiz-Lopez et al., 2007a) and radiation data (2π spectral radiometer, periodically inverted for upwelling flux).

An overview of the climatology of the Antarctic boundary layer at Halley during the CHABLIS campaign is presented elsewhere (Jones et al., 2007[2]); however the basic environmental conditions are summarised in Table 1, together with the broad chemical composition. The corresponding levels of CH_4 and H_2 at Halley in January/February 2005 were 1720 and 546 ppb respectively (NOAA Global Monitoring Division flask analyses). Note that Table 1 refers only to the summer period (January/February 2005) during which the HO_x instrument was deployed; similarly in the remainder of this manuscript the phrase "measurement period" refers to the days in January and February 2005 when HO_x measurements were performed.

3 Experimental approach

OH and HO_2 radicals were detected using laser-induced fluorescence, via the FAGE (Fluorescence Assay by Gas Expansion) methodology (Hard et al., 1984). The system has been described previously (e.g. Bloss et al., 2003; Smith et al., 2006); brief details and differences from previous campaigns are summarised here.

OH radicals were detected via on-resonance pulsed laser-induced fluorescence through the $A^2\Sigma^+ \leftarrow X^2\Pi_i$ (0,0) transition at approximately 308 nm. Ambient air was drawn through a 1.0 mm diameter flat nozzle into a 250 mm diameter fluorescence excitation chamber held at a pressure of approximately 0.9 Torr using a throttled Roots blower/rotary pump. The resulting expansion jet was intersected (approximately 120 mm below the nozzle) by the excitation laser

[1] Bloss, W. J., Lee, J. D., Heard, D. E., Saiz-Lopez, A., Plane, J. M. C., Salmon, R. A., Bauguitte, S. J.-B., Roscoe, H. K., and Jones, A. E.: Box Model Studies of Radical Chemistry in the Coastal Antarctic Boundary Layer, in preparation, 2007.

[2] Jones, A. E., Wolff, E. W., Salmon, R. A., et al.: Chemistry of the Antarctic Boundary Layer and the Interface with Snow: An overview of the CHABLIS campaign, Atmos. Chem. Phys. Discuss., in preparation, 2007.

Table 1. Chemical and Meteorological Conditions at Halley during the HO_x Measurement Period.

Basic Chemical Climatology					
Species:	NO/ ppt	NO_2/ ppt	CO/ pbb	O_3/ ppb	HCHO/ ppt
Min	<LOD	<LOD	17.2	5.3	3
Mean	8.1	4.8	34.5	8.8	131
Max	66.5	69.3	38.6	13.0	385

Notes: Values refer to filtered data only, i.e. excluding air from base sector which may include generator exhausts. Limit of Detection (LOD) for NOx: Conservatively 1.5 ppt for NO; 3–4 ppt for NO_2.

Meteorological Parameters				
Parameter:	Temp/ K	Pressure/ mbar	$j(O^1D)$/ $10^{-5}\,s^{-1}$	$H_2O/10^{16}$ molec cm^{-3}
Min	254.3	962.8	–	3.12
Mean	268.1	984.7	–	9.39
Max	275.0	994.0	4.04 [b]	1.66

Note b: $j(O^1D)$ value is maximum of hourly-binned data averaged over measurement period.

beam. OH LIF was detected along a perpendicular detection axis. A gas injection ring is positioned approximately 60 mm below the nozzle, permitting the addition of NO for the conversion of HO_2 to OH. The system can thus detect a signal due to ambient OH, or to the sum of OH + HO_2, with an empirically determined sensitivity.

The excitation radiation was provided by an all-solid-state laser system, comprising an intra-cavity doubled Nd:YAG pumping a Ti:Sapphire oscillator. The wavelength of the near-IR fundamental output of the Ti:Sapphire laser (924 nm) was selected using an adjustable grating, and then frequency tripled via two non-linear stages using a pair of CLBO crystals, firstly to generate the second harmonic at 462 nm, and then to perform sum-frequency mixing of this wavelength with the fundamental (924 nm) to obtain the desired 308 nm radiation. During the CHABLIS campaign, the laser system produced 30–50 mW of 308 nm radiation at 5 kHz pulse repetition frequency.

In normal operation the laser radiation is divided into three fractions, for OH, HO_2 and reference cells respectively; however during the CHABLIS campaign technical difficulties led to operation with a single fluorescence cell (and reference cell). The reference cell, into which a small fraction (5%) of the total laser power was directed, contained a relatively high concentration of OH generated from a microwave discharge through humidified air at reduced pressure. The signal from this cell provides a wavelength calibration and was used to lock the laser wavelength to a particular OH transition. A fibre optic cable was used to deliver the main fraction of the laser beam to the fluorescence cell, where the beam was collimated, and directed through baffled arms across the fluorescence cell. After traversing the cell, the beam was directed onto a filtered photodiode, the resulting laser power measurement used to normalise the fluorescence signal. Typical laser power in the fluorescence cell was 10–15 mW.

The detection axis comprised a quartz window, collimating lenses, interference filter (transmission >50% at 308 nm; FWHM 8 nm; very high rejection (transmission $<10^{-6}$) at other wavelengths) and focussing lenses, which directed the OH fluorescence onto the cathode of a channeltron photomultiplier tube (PMT). The solid angle of fluorescence collection was approximately doubled with a spherical mirror mounted opposite the collimating optics. The PMT was switched off immediately prior to and during the laser pulse using a gating circuit to apply a 100 V positive voltage to the cathode relative to the channeltron body. OH fluorescence was recorded by photon-counting during a 500 ns wide integration window, commencing 100 ns after the start of the laser pulse. The delay accounts for the laser pulse width (ca. 35 ns) and the PMT gating circuit time response (ca. 50 ns). A second integration window, delayed 50 μs after the laser pulse, was used to measure the signal arising due to scattered solar radiation through the nozzle, for subsequent subtraction.

For the Antarctic deployment, a new roof enclosure was constructed to house the sampling cells, pressure control and electronic gating boxes on top of the container. The roof enclosure was thermostatically heated to 15°C throughout the measurement campaign. Additional modifications for the Antarctic deployment included a heated external calibration unit, and extended exhaust line, incorporating a combined sofnofil/activated charcoal scrubber, which vented into a buried snow pit ca. 50 m downwind of the measurement site.

Data cycle

Due to instrumental difficulties, only a single measurement cell was operable during CHABLIS, which was used to perform alternating measurements of OH and (OH + HO_2). Data were acquired as 5×30 s duration averages of the OH signal, followed by 5×30 s averages of the OH + HO_2 signal (NO turned on), followed by 4×30 s averages of the background (offline – dark counts and residual laser scatter). All points were corrected for solar scatter on a second-by-second timescale as described above. The instrument duty cycle was ca. 8 min (including wavelength adjustment periods). The data were subsequently converted to 10 min averages for comparison with other measurements.

4 Calibration

LIF is not an absolute technique, thus calibration of the instrument response factor is required; during CHABLIS, the system was calibrated using the water photolysis / ozone actinometry approach (Aschumtat et al., 1994) to determine the response factor C relating the measured signal S to the OH or OH + HO_2 volume mixing ratio (vmr) at a given laser power P_{wr} :

$$S = C \times P_{wr} \times (\text{OH or OH} + HO_2 \text{ vmr}) \quad (1)$$

The calibration source consists of a 22 mm internal diameter by 400 mm length quartz tube, through which 12 slm (standard litres per minute) of humidified air was flowed, under approximately laminar conditions. The 184.9 nm radiation from a mercury "pen-ray" lamp was used to photolyse the water vapour and oxygen within the tube, in an irradiation zone approximately 20 mm from the sampling nozzle, leading to the generation of OH, HO_2 and O_3. The mercury lamp output was filtered using a 184.9 nm bandpass filter before passing through the calibration flow. The calibration unit housing was purged with a flow of N_2 to prevent absorption of the lamp output by oxygen in ambient air, and ozone build-up. For HO_2 calibrations, an additional flow of CO (25 sccm) was added to the humidified air flow before the calibration tube, to convert the OH formed to HO_2.

After passing the photolysis region the calibration flow impinges upon the nozzle of the LIF system, and a fraction of the total flow (ca. 5 slm) is drawn into the instrument. The remainder of the flow is directed to an ozone monitor, dew point hygrometer and subsequently vented. As the humidity of the air entering the flow reactor is known the concentration of OH or HO_2 radicals formed can be calculated from the measured ozone concentration and the relevant cross sections and quantum yields.

A complication arises due to the radial distribution of the axial flow velocity within the laminar flow tube: Air in the centre of the tube travels faster than air at the edges, and so spends less time in the photolysis region, and thus has lower OH, HO_2 and O_3 concentrations. The LIF nozzle samples from the centre of the flow tube, while the ozone concentration measured is the average of the remaining flow – a correction (the profile factor, P) must therefore be applied. For perfect laminar flow, with a parabolic velocity profile, and zero sample withdrawal by the LIF nozzle, the correction would be a factor of 2; for the calibration system used a value of P=(1.92±0.05) was measured.

The OH present at the LIF system sampling nozzle can then be calculated via Eq. (2):

$$\text{HOx/ppt} = \frac{(O_3/\text{ppt}) \times (H_2O/\text{ppt}) \times \sigma_{H_2O} \times \Phi_{HOx}}{2.08 \times 10^{11} \times P \times \sigma_{O_2} \times \Phi_{O_3}} \quad (2)$$

where Φ_{O3} is the quantum yield for the (ultimate) production of O_3 from oxygen photolysis, equal to 2 (Washida et al., 1971) and Φ_{HOx} is the quantum yield for production of OH or HO_2 following water photolysis, equal to 1 (for OH in the absence of CO) or 2 (for HO_2 in the presence of CO) (Sander et al., 2006). 2.08×10^{11} is the atmospheric volume mixing ratio of oxygen (in ppt), P is the profile factor referred to above, and $\sigma(H_2O)$ and $\sigma(O_2)$ are absorption cross sections for water and oxygen (respectively) at 184.9 nm. A value of $(7.1\pm0.2) \times10^{-20}$ molecule^{-1}cm^2 was used for $\sigma(H_2O)$, being the mean of the determinations of Cantrell et al. (1997), Hofzumahaus et al. (1997) and Creasey et al. (2000). A value of $\sigma(O_2)$=(1.25±0.08) $\times10^{-20}$ molecule^{-1}cm^2 was determined for the pen-ray lamp used during the CHABLIS campaign, under the actual operating conditions of oxygen column, lamp current and cooling flow employed in the calibration system. The use of the mixing-ratio version of the calibration equation (E2, as shown) rather than its number-density equivalent avoided complications arising from small temperature and pressure differences between the O_3 and H_2O monitors within the container, the external calibration cell, and ambient air. The calibrations were performed in zero air, produced by passing ambient air through a pure-air generator which incorporated freeze-drying, heated catalyst VOC decomposition, NO to NO_2 conversion and charcoal scrubbing stages. The resulting zero air was re-humidified as desired using snow melt purified through a Millipore system. CO (Sigma-Aldrich, 99%) and NO (Air Products, 99%) were used as supplied.

The OH LIF signal is expected to decrease with increasing humidity in the sampled air, as H_2O is an extremely efficient quencher of electronically excited OH radicals; the sensitivity of ambient HO_x LIF systems is however known to show a stronger dependence upon humidity than can be accounted for by quenching alone, in a manner dependent upon the precise sampling geometry (nozzle diameter, shaping; cell design) employed (Creasey et al., 1997). During the CHABLIS campaign, ambient humidity varied between 0.11% and 0.65% (dew points of –19.4 to +0.4°C respectively). Calibrations were therefore performed as a function of humidity. Calibrations at a range of water levels were performed every 3 days on average (11 times in total over the 39 days of measurements), and all calibration data were averaged to determine a mean (humidity dependent) instrument sensitivity for the campaign, which was applied to all the measured data. Figure 1 shows the humidity dependence of the determined calibration constants C for OH and HO_2. Fewer HO_2 calibrations were performed due to a limited supply of CO. Under the median conditions of 0.4 % absolute humidity (dew point –5.2°C), the instrument sensitivity was 17 counts s^{-1} mW^{-1} ppt^{-1} for OH and 1.2 counts s^{-1} mW^{-1} ppt^{-1} for HO_2, corresponding to typical detection limits of 4.8×10^{-3} and 0.068 ppt (ca. 1.3×10^5 and 1.8×10^6 molecules cm^{-3}) respectively, in (just under) 5 min. The difference in OH and HO_2 sensitivity reflects the low conversion efficiency achieved under the configuration (nozzle diameter; NO injector arrangement; NO flow) used during CHABLIS.

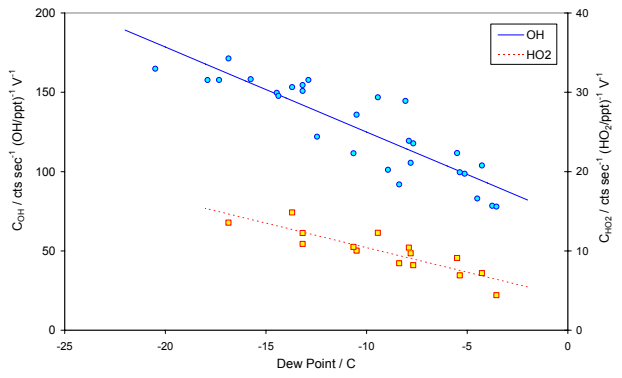

Fig. 1. Calibration constants for OH (blue circles) and HO_2 (red squares) measured during the campaign, as a function of humidity. Lines indicate linear regressions used to analyse the ambient HO_x data. The data are given in terms of laser power in the fluorescence cell, measured via UV photodiode, and can be converted approximately into units of counts s^{-1} $(HO_x/ppt)^{-1}$ mW^{-1} by dividing by 6.

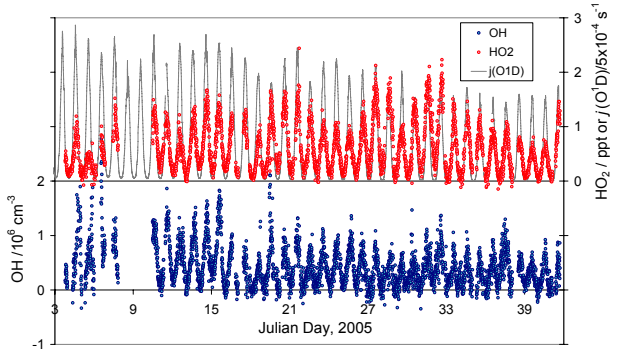

Fig. 2. Time series of OH (molecule cm^{-3}; blue) and HO_2 (ppt, red, upper panel) data for the campaign, together with $j(O^1D)$ (s^{-1}; black line, upper panel).

The overall uncertainty in the HO_x levels determined via Eq. (2), and hence the instrument calibration, can be calculated from the uncertainty in the individual factors. Systematic uncertainties in the values of the water and oxygen cross sections, the profile factor and the accuracy of the ozone analyser and dew-point hygrometer give an uncertainty of 22% when combined in quadrature. To this must be added the precision in the ozone and water measurements, which largely accounts for the scatter apparent in Fig. 1, and which we estimate to be 15%, giving a combined uncertainty for this campaign of 27%. As in practice the average of multiple calibrations was used to analyse the HO_x data (i.e. the regression lines shown in Fig. 1), this value may over estimate the total uncertainty, although naturally only known sources of error are taken into account. Interference tests were performed during the campaign, in which C_3F_6 was added to the calibration flow, resulting in the removal of all OH radicals (Dubey et al., 1996); the instrument signal fell to background levels. No signal was observable when the NO flow was turned on (during calibration, with the mercury lamp off, i.e. in the absence of any OH or HO_2 radicals), indicating that any HO_2 artefact (arising from, for example, HONO and/or HNO_3 formation in the NO supply line, both of which may photolyse in the laser pulse to form OH) was below detectable levels. The NO titration flow was replaced with N_2, and turned on/off during normal calibration, with no change in the detected OH signal, indicating that flow disturbance in the cell arising from the gas injection was negligible.

5 OH and HO_2 observations

Figure 2 shows the entire OH and HO_2 dataset obtained at Halley, together with $j(O^1D)$ as determined by a spectral radiometer. HO_x data were recorded on 37 days between 3 January and 10 February 2005, including a near-unbroken 5-week spell from 11 January – the instrument was shut down as blizzard conditions prevented access to the measurement site over the 8–10 January period. The campaign yielded slightly over 4000 10-min averaged OH and HO_2 data points.

As Fig. 2 shows, OH and HO_2 followed a diurnal profile very closely coupled to the variation in photolysis rates. HO_x levels were above zero even at their lowest levels – as Halley lies within the Antarctic circle, 24 h daylight is present during January and early February (maximum solar zenith angle of 82°–89°; 11 January–13 February – for comparison, the minimum values $j(O^1D)$ and $j(NO_2)$ "at night" were 2.6 % and 11.4 % of their maximum values, on average over the measurement period). A seasonal cycle is clearly visible in the $j(O^1D)$ and OH data, with maximum and minimum values decreasing towards the end of the measurement period as solar zenith angles increased. The trend is less clear in HO_2, reflecting both the more complex HO_2 production and removal chemistry, and the natural buffering of HO_2 levels which results from self-reaction accounting for a significant fraction of their removal.

The OH and HO_2 levels were observed to respond to local (base generator exhaust) pollution events: Figure 3 shows the response of HO_x to an NO spike experienced at the measurement location, as the local wind direction veered from westerly to easterly in a clockwise manner (through North), bringing exhaust from the base generators, containing NO_x, over the measurement site at approximately 9 am on 30 January. OH levels rise and HO_2 levels fall in response to the NO_x perturbation. Note the data shown are 10-minute averages, thus the fine structure in the NO and HO_x variation is obscured. The remainder of the day shows a diurnal cycle in radical levels in response to solar radiation.

No obvious correlations with local meteorology were observed for the HO_x levels other than the variations with photolysis rates, temperature, humidity etc. which would be expected. In particular, no dependence upon wind direction

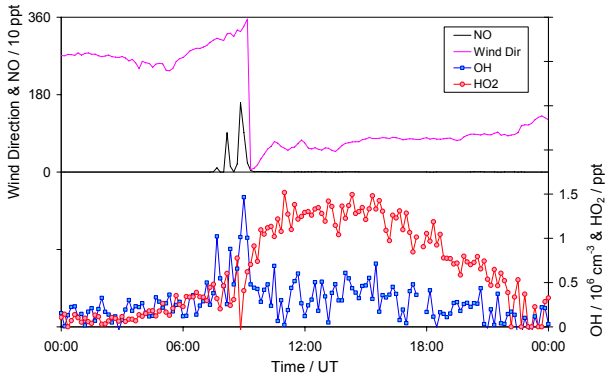

Fig. 3. HO_x perturbation due to base pollution event of 30 January. Time series of OH (red circles, 10^6 molecule cm^{-3}) and HO_2 (blue circles, ppt) (lower panel), together with NO (black line, ppt/10) and local wind direction (pink line) (upper panel).

(within the clean air sector) or wind speed was observed, which contrasts with the elevated levels of OH reported at high wind speeds for Summit, Greenland (Sjostedt et al., 2005). On several occasions, local radiation fog was observed to form, usually in a layer a few metres thick encompassing the inlet height for the LIF system. During these events, radical levels fell below the detection limit.

The raw data were filtered to exclude air from the base air sector (local wind directions from 290° to 345°) or during very low wind speeds ($<1\,ms^{-1}$), when recycling of air from the CASLab exhaust could have occurred. Of the remaining measurements (90.0% of the total), the mean OH concentration was $3.9\times10^5\,cm^{-3}$, with mean maximum and minimum values of $7.9\times10^5\,cm^{-3}$ and $8.2\times10^4\,cm^{-3}$ (maximum/minimum values of the mean level, for each hour of the day, averaged over the whole campaign). The corresponding mean HO_2 mixing ratio was 0.76 ppt, with maximum and minimum levels of 1.50 and 0.18 ppt respectively. Figure 4 shows the mean and single standard deviation for all (filtered) values of OH and HO_2, in hourly bins.

6 Empirical relationship to photolysis rates

Photolysis of various precursor species ultimately determines the rate of production of HO_x and, as a consequence of the relatively short and constant OH and HO_2 lifetime, is strongly related to HO_x concentrations. Observed OH and HO_2 levels can therefore frequently be expressed as relatively simple functions of photolysis rates, which can provide both a convenient parameterisation for the HO_x levels in a particular environment, and an insight into the chemical processes controlling their abundance.

The dependence of OH levels upon the rate of production of electronically excited oxygen atoms, $j(O^1D)$, depends upon the chemical environment: In the absence of NO_x and

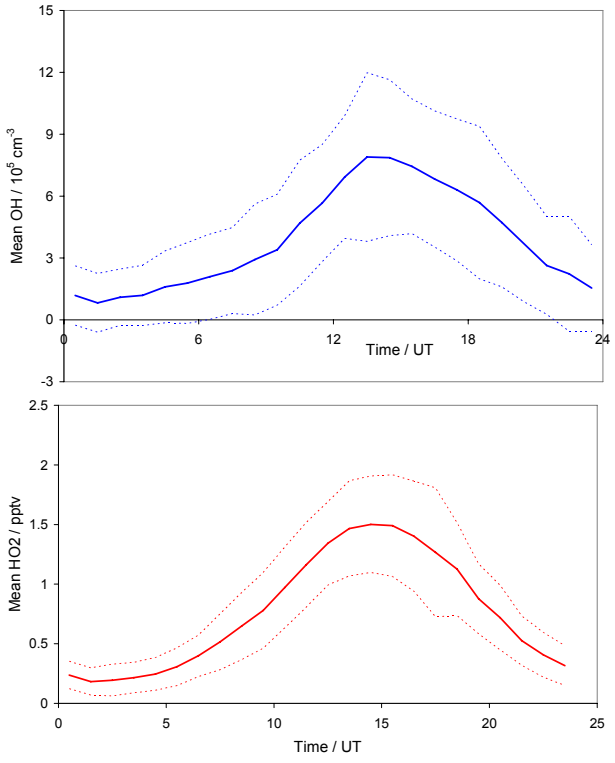

Fig. 4. Hourly mean values of **(a)** OH and **(b)** HO_2 observed during the campaign, together with ±1 standard deviation values. Data filtered to exclude base pollution as described in the text.

halogen species, primary production via reactions R1 and R2 is expected to dominate, and OH is expected to show an approximately linear relationship with $j(O^1D)$, with some deviation due to $HO_2 + O_3$ and H_2O_2 photolysis. At higher NO levels, or in the presence of halogen oxides (XO), processes such as the HO_2 + NO reaction, HO_2 + XO and HONO photolysis are of increasing importance and the relationship between OH and $j(O^1D)$ becomes more complex. In their analysis of OH data acquired at a rural site in Germany, Ehhalt and Rohrer (2000) have shown that for a particular NO_x level the dependence of OH upon $j(O^1D)$ can be better described by an expression of the form $OH = a\times j(O^1D)^b$, where the non-unity exponential parameter incorporates the influences of (e.g.) $j(NO_2)$ and j(HONO) upon OH production, via HO_2 + NO and HONO photolysis respectively. Subsequently the addition of an intercept, allowing for non-photolytic radical sources (e.g. NO_3 chemistry or alkene ozonolysis) has been shown to improve the correlations in some environments (Smith et al., 2006). HO_2 can also be parameterised in terms of $j(O^1D)$; in the absence of NO_x (or XO species), peroxy radical levels are expected to be approximately linearly related to $j(O^1D)^{1/2}$ (Penkett et al., 1997). With increasing NO_x (or XO), radical cycling from RO_2 to HO_2 and HO_2 to OH becomes more significant, and the exponent may increase or decrease.

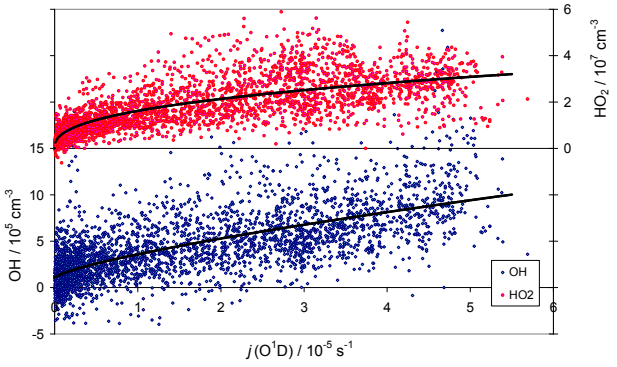

Fig. 5. Variation of clean-air sector OH and HO_2 data with $j(O^1D)$, together with fits to Eq. (3).

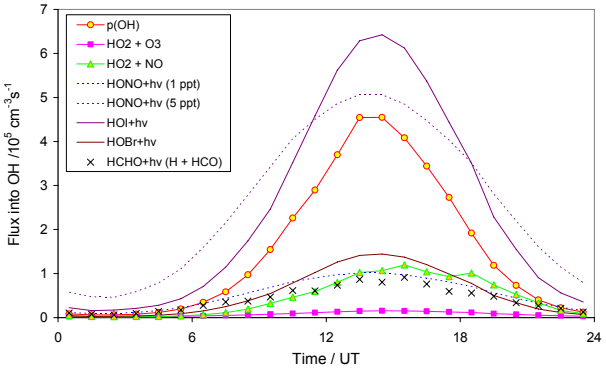

Fig. 6. Calculated mean diurnal variation of principal OH production mechanisms over the measurement period; see text for details. p(OH) indicates primary OH production through ozone photolysis.

At Halley in summer, while NO levels are low (relative to the moderately polluted sites considered by Ehhalt and Rohrer), the halogen oxides make a significant contribution to OH production via photolysis of HOI and/or HOBr, and HCHO photolysis contributes significantly to the production of HO_2 (see below). We therefore expect some deviation from a linear dependence of OH upon $j(O^1D)$. The dependence of the OH and HO_2 observations upon $j(O^1D)$ was investigated by fitting Eq. (3), below, to each dataset:

$$X = a \times \{j(O^1D)/10^{-5}\,s^{-1}\}^b + c \quad (3)$$

where X = OH/10^5 molecule cm^{-3} or X = HO_2/10^7 molecule cm^{-3}. The resulting values of a, b and c are summarised in Table 2, together with comparisons to the equivalent parameters reported for other environments, and are shown on Fig. 5.

7 OH production, removal and steady state analysis

In this section the observed OH levels are compared with values predicted using simple steady-state calculations. These calculations neglect (for example) reaction of OH and HO_2 with intermediates in the degradation of VOCs, and production of HO_x through the photolysis of carbonyl intermediates; nonetheless they serve to indicate the key features of the atmospheric chemistry. A full model simulation, including integrated HO_x-NO_x-XO chemistry, is the subject of a separate manuscript (Bloss et al., 2007[1]).

OH production

Figure 6 shows the mean OH production rates over a diurnal period, obtained from an average of all filtered data over the measurement period, for ozone photolysis, reaction of HO_2 with O_3 and with NO, and photolysis of HONO at constant levels of 1 and 5 ppt. Also shown for comparison is the rate of production of HO_2 from the H + HCO channel of formaldehyde photolysis. Kinetic and photochemical parameters from Sander et al. (2006) were used. OH production from hydrogen peroxide formation is not shown (for clarity) – the mean level of H_2O_2 observed during the measurement period was 79 ppt (Walker et al., 2006), which would give rise to photolytic OH production equivalent to approximately half that shown for 1 ppt of HONO on Fig. 6.

The DOAS system described earlier detected the halogen oxides IO and BrO at Halley during the CHABLIS campaign (Saiz-Lopez et al., 2007a). During the summertime period (January/February 2005), IO was observed to follow a diurnal profile with average mixing ratios ranging from approximately 0.7 ppt to 5.5 ppt. BrO levels were comparable. The halogen monoxide radicals were detected in most DOAS spectra (of the appropriate wavelength region) indicating that they are likely to have been present most of the time, and to significantly affect the boundary layer radical chemistry. IO and BrO will affect HO_x levels through a number of processes, most significantly (from the perspective of performing steady-state OH calculations) by converting HO_2 to OH via formation of HOI and HOBr, which may then undergo photolysis, heterogeneous loss or reaction with OH :

$$HO_2 + XO \rightarrow HOX + O_2 \quad (R12)$$

$$HOX + h\nu \rightarrow OH + X \quad (R13)$$

$$HOX + \text{aerosol} \rightarrow \text{loss} \quad (R14)$$

$$HOX + OH \rightarrow H_2O + XO \quad (R15)$$

The contribution of halogen-mediated $HO_2 \rightarrow$OH conversion can be approximately calculated by assuming HOI / HOBr are in steady state defined by reactions R12-R14:

$$[HOX]_{ss} = k_{12}[HO_2][XO]/(j_{13} + k_{14}) \quad (4)$$

Aerosol loss of HOI and HOBr is likely to be significant (Bloss et al., 2005); however the reaction probability is poorly known and unfortunately no aerosol surface

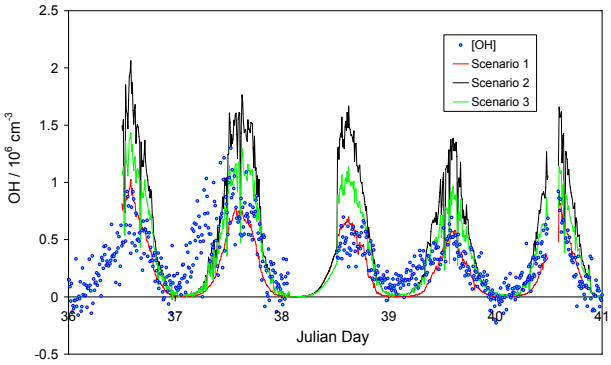

Fig. 7. Measured OH concentrations for 6–10 February 2005, days 36–40, together with calculated steady-state levels; see text for details.

area measurements were available during CHABLIS. We have calculated the contribution of HOI photolysis to OH production, via Eq. (4), assuming an aerosol surface area of 1×10^{-7} cm^2 cm^{-3} (Davison et al., 1996) and a reaction probability of 0.2 for both HOBr and HOI. (k'_{uptake} calculated using the free molecular approximation). HOI photolysis is approximately 200 times faster than heterogeneous loss under these assumptions at midday, and about 5 times faster at the maximum solar zenith angle; thus the impact of errors in the aerosol parameters assumed upon calculated OH is small for much of the day. Reaction of HOX with OH can be neglected (the relative rates of Reactions R13 and R15 at noon under the conditions at Halley were 247:1 for HOI). The resulting OH production rates are also shown on Fig. 6.

OH removal

Considering the species measured during CHABLIS, OH removal was dominated by reaction with CO (54.2%), CH_4 (33.0%), and H_2 (8.9%), with smaller contributions from DMS, alkenes (iso-butene, propene, ethene), H_2O_2, NO_2 and ethane (all 0.03–1%). Methanol was not measured, but anticipated levels (200 ppt, Jacob et al., 2005) would correspond to a 0.4% contribution to OH loss. Of the measured species, OH removal is clearly dominated by CO and CH_4. The impact of methane is reduced compared with boundary layer locations at lower latitudes due to the strong temperature dependence of the OH + CH_4 rate coefficient, E/R = 1775 K (Sander et al., 2006). The measured sinks correspond to a mean OH (e^{-1}) lifetime of 2.1 seconds during the measurement period.

No measurements of oxygenated VOCs (other than formaldehyde) were available during CHABLIS. Higher aldehydes have been observed in the Arctic boundary layer (Boudries et al., 2002), and in conjunction with firn air observations suggest a net snowpack source to the overlying atmosphere (Guimbaud et al., 2002), potentially originating

Table 2. Parameters for empirical fits of OH and HO_2 levels to $j(O^1D)$ via Eq. (3).

Fitting Eq. (3) to all OH data				
Fit	*a*	*b*	*c*	r^2
1 *Linear*	2.22±0.02	1 (fixed)	0 (fixed)	0.38
2 *Power*	3.89±0.06	0.51±0.01	0 (fixed)	0.46
3 *Power/Intercept*	2.52±0.16	0.74±0.04	1.06±0.12	0.48
Calculated OH	4.66±0.09	0.63±0.02	0±0.1	–
Fitting Eq. (3) to all HO_2 data				
4 *Power*	1.61±0.01	0.40±0.01	0 (fixed)	0.60

Notes: Uncertainties are ±1 s.d. Calculated OH refers to the fit obtained from OH levels calculated under scenario 3.

Literature values for OH and HO_2–$j(O^1D)$ parameterisations			
	a	*b*	*c*
OH			
Brauers et al. (2001) ALBATROSS, Tropical Atlantic	13.7	1 (fixed)	0 (fixed)
Holland et al. (2003) BERLIOZ – Rural Germany	20[1]	1 (fixed)[1]	0 (fixed)[1]
Smith et al. (2006) NAMBLEX, Mace Head, Ireland	14.7	0.84±0.05	4.4
Rohrer and Berresheim (2006) Hohenpeissenberg Observatory	24	1	1.3
Berresheim et al. (2003) MINOS (Coastal Crete)	72	0.68	1
HO_2			
Holland *et al.* (2003) BERLIOZ (low NO)	20[1]	1 (fixed)[1]	0 (fixed)[1]

Notes: Uncertainties are ±1 s.d. Values from literature sources have been adjusted to be in terms of $OH/10^5$, rather than 10^6, for consistency. 1: Estimated from figures in manuscript (values not given).

from the organic matter within snowpack. Laboratory experiments have shown similar production of acetaldehyde from South Pole snow (Grannas et al., 2004), thus a similar mechanism might be expected to operate in other, related environments, i.e. at Halley. Acetaldehyde and other carbonyl species would affect the local radical chemistry, both through photolysis leading to radical production, and through direct reaction with OH providing an additional OH sink. For example, if acetaldehyde was present at the levels observed in the Arctic (29–459 ppt during the 24-h daylight period – Boudries et al., 2002), the total OH sink would be increased by between 3 and 48%, giving a considerable reduction in the OH lifetime.

Steady-state OH levels

Figure 7 shows a 5-day period (Julian days 36–40) of measured OH concentrations, and steady-state OH levels calculated according to the three scenarios listed below, described in more detail in the following section:

1. Production from O_3 photolysis and the reactions of HO_2 with NO and O_3

   Loss due to reaction with all measured sinks

2. As 1 but with additional OH production due to HOI photolysis

3. As 2 but with an additional OH sink: Reaction with acetaldehyde

Scenario 1 reflects the conventional tropospheric chemistry which might be expected for a remote location.

Scenario 2 allows a semi-quantitative investigation of the impact of the halogen oxides, IO and BrO, upon OH levels. IO and BrO absorb in different wavelength regions, thus no simultaneous observations of both halogen monoxides were possible from the DOAS. The IO dataset is the more extensive of the two during the HO_x measurement period (more time was spent measuring IO than BrO), consequently the IO data has been used here as a proxy for the total impact of XO (IO and BrO) upon HO_x. The IO dataset is itself limited compared with the OH observations, consequently IO levels were calculated from a purely empirical relationship between the DOAS IO observations over the summer period and the corresponding measurements of $j(NO_2)$, which were found to be highly correlated:

$$\mathrm{IO/ppt}=(j(\mathrm{NO_2})/\mathrm{s} \times 280) + 0.7 \quad (5)$$

HOI was assumed to be in steady state, defined as described by Eq. (4).

Scenario 3 considers the likely possibility that further, unmeasured VOCs are present and provide additional OH sinks. An additional OH sink was added to the calculation, equal in magnitude to 167 ppt of acetaldehyde (on average), varying diurnally with $j(NO_2)$ – selected to replicate the CH_3CHO observations reported in the Arctic (Boudries et al., 2002). In addition to scenarios 1–3, further production of OH might also be expected to result from HONO photolysis; this possibility is examined in the Discussion section.

8 Discussion

The OH levels measured in coastal Antarctica during the CHABLIS campaign are reasonably consistent with those observed at Palmer Station on the Antarctic Peninsula (Jefferson et al., 1998), but are considerably lower than those observed at South Pole (Mauldin et al., 2001, 2004). The mean HO_2 level observed at Halley is also rather lower than $HO_2 + RO_2$ levels observed at South Pole during ISCAT2000 (Mauldin et al., 2004), by a factor of 3–4. The Halley HO_2 levels are however higher than those observed at Summit, Greenland (by a factor of 3 for the summer campaign) – (Sjostedt et al., 2005).

The contrast between the HO_x levels at Halley and the higher levels at South Pole can be explained largely by the effect of the low mixed layer height at South Pole amplifying the effect of snowpack emissions of NO_x (Davis et al., 2004), HCHO and H_2O_2 (Chen et al., 2004) resulting in NO levels averaging 100–200 ppt. At such levels, NO dominates HO_x cycling and OH levels, and the effects of halogen species upon HO_x levels would be small; moreover boundary layer halogen levels are expected to be negligible at the pole. Daytime boundary layer heights of 100 m have been inferred for Halley during the CHABLIS campaign (Anderson, 2006). It is also worth noting that the South Pole site received near-uniform sunlight around the solstice, while Halley experiences a significant diurnal cycle (Fig. 2). Observations of nitrous acid, HONO, were also reported from South Pole during the ISCAT2000 campaign (Dibb et al., 2004), with mixing ratios of around 30 ppt measured using a mist chamber/ion chromatography technique. HONO photolyses rapidly in the boundary layer, with a lifetime of a few minutes (250 s at noon during CHABLIS on average), thus ppt levels of HONO would make a large contribution to the HO_x budget. Modelling studies were unable to reconcile the HO_x and NO_x levels observed at South Pole with the HONO observations (Chen et al., 2004). Subsequently, HONO measurements were performed at South Pole during the December 2003/January 2004, using both mist chamber/ion chromatography and LIF approaches. The LIF system detected HONO at levels of around 6 ppt, sufficient to form a major source of HO_x, but lower than the concurrent mist chamber observations by a factor of 7 (Liao et al., 2006).

HONO measurements were also performed during CHABLIS: measurements were performed by stripping to the aqueous phase in a glass coil chamber, followed by a complexation/diazotization reaction to produce an azo dye detectable by absorption spectroscopy (Clemitshaw, 2004). The mean HONO level observed during the HO_x measurement period at Halley was 7 ppt (Clemitshaw, 2006 and personal communication). At such levels, HONO photolysis would dominate the HO_x budget – Fig. 6 shows the OH production rates which would result from constant levels of 1 and 5 ppt HONO. This would lead to the HO_x steady-state levels far exceeding the observations, even in the hypothesised presence of additional oxygenated organic species contributing to the total OH sink. The NO production resulting from HONO photolysis would also lead to calculated NO_x levels far greater than those observed – The mean NO_x level at Halley during the HO_x measurement period was 15 ppt (Bauguitte et al., 2005) with a lifetime of approximately 6 h (consistent with heterogeneous hydrolysis of halogen nitrates). This can be compared with the HONO photolytic

lifetime of approximately 4–10 min, indicating that a few ppt of HONO would be expected to produce much higher NO_x levels. In common with the earlier South Pole studies, we cannot currently reconcile the HO_x and NO_x observations with the observed HONO data, without invoking a large unidentified additional HO_x and NO_x sink. A positive artefact in the HONO data could explain this discrepancy: The technique in practice detects total soluble nitrite, thus contributions from aerosol, from peroxynitric acid, or from the halogen nitrite species INO_2 and $BrNO_2$, could contribute to the measured signal - however the concentrations of the latter are calculated to be a fraction of a ppt under the conditions prevalent at Halley.

The presence of significant levels of halogen activity was confirmed during CHABLIS by the DOAS observations of IO and BrO (Saiz-Lopez et al., 2007a). Due to the nature of the DOAS system, the halogen observations were less frequent than the HO_x data during the summer period; however IO was detected during every attempted observation, at levels which were well described by Eq. (5). It is therefore likely that both iodine and bromine species were present in the boundary layer at Halley throughout the summer campaign, with a number of impacts upon the chemical composition: As described above, the halogens act to drive the radical cycling from organic peroxy radicals to HO_2 to OH, with concomitant ozone destruction due to the reformation of halogen atoms. Additional ozone destruction will also result from the halogen oxide cross- and self-reactions, IO + IO, IO + BrO and BrO + BrO. Further, the halogens will change the NO_x partitioning (through the IO + NO and BrO + NO reactions), and provide an additional NO_x sink, through formation and the subsequent deposition or heterogeneous loss of halogen nitrates. (The calculated halogen nitrate sink reduces the NO_x lifetime to around 6 h, insufficient to reconcile NO_x levels with the NO production that would result from photolysis of the observed levels of HONO – Bauguitte et al., 2006). Reaction with IO and with BrO forms the dominant sink for HO_2 and source of OH. Production of HI and HBr are likely to add to the HO_x sink. Peroxy radical levels may be increased due to elevated OH levels and reductions in HO_2, but this effect will be offset by the RO_2 + XO reactions, depending upon the kinetics employed. The full impacts of the halogen species are considered in the detailed box and 1-dimensional model studies reported elsewhere (Bloss et al., 2007[1]; Saiz-Lopez et al., 2007b).

The observed levels of OH were reproduced reasonably well by steady-state OH levels calculated under scenario 1 (Fig. 7), with a calculated:observed ratio of 0.67, reflecting conventional remote tropospheric chemistry disregarding the effect of halogens and HONO, are in good agreement with the observations. However, HOBr and (particularly) HOI photolysis will lead to additional OH production, and to a significant over-prediction of the measured OH levels (scenario 2, mean calculated:observed ratio = 1.64). While the IO present on a given day may well have been less than that assumed through Eq. (5), scenario 2 neglects the additional HO_2 to OH conversions anticipated through HOBr formation and photolysis, i.e. the impact of BrO. Observed BrO levels were comparable with those of IO (Saiz-Lopez et al., 2007a), on which basis the contribution of HOBr photolysis to OH formation is anticipated to be approximately 4 times smaller than that of HOI (due to the lower BrO+HO_2 rate constant and HOBr cross sections). Addition of a further OH sink would improve the agreement: The hydrocarbon measurements during CHABLIS (C2-C6 alkanes, alkenes and aromatics) notably excluded oxygenated hydrocarbons (other than HCHO), which react reasonably rapidly with OH and have been shown to form a significant portion of the total radical sink in the marine boundary layer (Lewis et al., 2005). Acetaldehyde, acetone and other oxygenated VOCs were observed during ALERT in the Arctic (Boudries et al., 2002) indicating that such compounds can reach appreciable concentrations in the polar boundary layer environment; whether such levels are also found in the Antarctic, considerably further removed from anthropogenic emission sources, is less certain, although we note that studies have reported comparable total organic carbon content in snow samples from South Pole, Summit (Greenland) and Alert (Grannas et al., 2004). Inclusion of an additional OH sink, equal in magnitude to that which would result from acetaldehyde present at the levels observed in the Arctic boundary layer, largely restores agreement between calculated and observed OH levels (scenario 3, calculated:observed ratio = 1.27).

Figures 6 and 7 show that the halogen oxides will dominate the radical cycling, compared with NO_x. The environment at Halley is thus one in which rapid radical cycling occurs, with a large chain length, but driven by XO rather than NO, and with associated ozone destruction rather than ozone production. This is in contrast with the situation in much of the troposphere, where minimal radical cycling, short chain lengths and very low NO_x levels are associated with (photolytic) ozone loss, and longer chain lengths are associated with elevated NO_x and ozone production.

The HO_2:OH ratio at Halley is 49.2 (mean local solar noon value), with a median value from all (filtered) HO_x data of 37.4. These values can be compared with ratios of 44–104 observed in the Southern Ocean boundary layer in Tasmania (Creasey et al., 2003), 76 in the Western Pacific (Kanaya et al., 2001) and 90-137 during in the pacific free troposphere (Tan et al., 2001). Conventional tropospheric chemistry predicts that under clean conditions (low NO), the ratio should increase as radical levels fall (due to the non-linearity in HO_2 loss through self-reaction), and should decrease as NO levels increase (due to HO_2 to OH conversion); upon this basis the observed HO_2:OH ratio might be expected to be higher than the other determinations listed above (clean conditions; low radical levels). However in the case of the Halley data, radical cycling is affected by the halogen species – the low HO_2:OH ratio for Halley, under low NO_x conditions, is indicative of efficient cycling of HO_2 to OH through reaction

with IO and BrO. The low values of the HO_2:OH ratio, which is a particularly robust measurement product as many of the instrumental and calibration factors cancel out, further demonstrates the importance of halogen-HO_x coupling in this environment.

OH and HO_2 vs. $j(O^1D)$ power dependencies

The OH and HO_2 data are reasonably well described by Eq. (3) in Fig. 5, reflecting the fact that the main processes dominating OH and HO_2 concentrations (photolysis of O_3, HCHO, H_2O_2; NO_x levels; XO levels) exhibit a strong and similar dependence upon solar irradiation. The OH data are best described by the full version (3) of Eq. (3). The positive intercept may reflect a contribution from radical production through photolysis routes with a broader SZA dependence than $j(O^1D)$ - for example HCHO or HONO. That the exponent b is less than unity is probably related to the role of halogen chemistry in driving the HO_x cycling, having a qualitatively similar effect to NO_x and reducing the direct dependence of OH upon $j(O^1D)$. The HO_2 data is well-described by the fit shown – addition of the intercept parameter (c) gave no significant improvement. The parameters may be compared with those obtained for measurements performed elsewhere which are also given in Table 2. The much larger OH concentrations observed in mid-latitudes are reflected in the higher value of the a coefficient, by a factor of up to 35. The similarity in the exponent b, 0.84 (Mace Head) and 0.68 (Crete) vs. 0.74 (Halley) indicates that the processes modifying the radicals' response to the sunlight levels, such as response to long- and short-wavelength components, are similar – possibly reflecting NO_x response at Crete, combined NO_x/halogen impacts at Mace Head, and halogen impacts at Halley. The higher value for parameter c, which indicates non-photolytic radical production, probably reflects the role of ozone-alkene and NO_3 initiated reactions at Mace Head, which would be much less significant at Halley (low O_3; low VOC levels; permanent (long-wavelength) illumination (summer) photolysing NO_3) – although a lower value than that recorded for Hohenpeissenberg might therefore also be expected; it is not clear why this is not the case. The expressions derived to relate the OH and HO_2 levels to $j(O^1D)$ may be used to roughly estimate the seasonal levels of OH and HO_2, from variations in actinic flux (assuming the summertime conditions and composition are typical of the rest of the year). Such a calculation is shown in Table 3 – these values were determined using the radiative transfer model TUV (Madronich and Flocke, 1998) to calculate the 24-hour average clear-sky $j(O^1D)$ level at the mid-point of each calendar month, scaling these values by comparing the January result to the actual, observed $j(O^1D)$ value and applying Eq. (3) to determine the OH/HO_2 level. Ozone columns were monthly averages over the period 1999-2004 for Halley. Such a calculation makes a number of assumptions, including that the summer chemistry is representative of the rest of the year, that chemical processes dominating the radical levels are linearly dependent upon $j(O^1D)$, and that the solar attenuation (cloudiness / weather) during January 2005 was typical of the rest of the year, but provide an indication of the annual HO_x levels in this environment. This approach produces mid-winter values of OH (May–July) which are likely to be overestimates (arising from the intercept parameter (c) in Eq. (3)), shown in parentheses in the table. The resulting annual mean OH concentration in the coastal Antarctic boundary layer is found to be 2.4×10^5 molec^{-1} cm^3. This value is lower than the global tropospheric mean OH concentration of $(9.8\pm1.6)\times10^5$ cm^{-3} (Bloss et al., 2005b), as expected given the low (annual average) light levels, absolute humidity etc. The annual trend in OH levels shown in Table 3 mirrors the seasonal variation in ethane and propane levels observed by GC measurements during the year-long CHABLIS observations (Read et al., 2007). The low winter/early spring values for OH (August/September) support the inference drawn by Read et al. (2007) that halogen chemistry (Cl and/or Br reactions) was responsible for shorter timescale variations in hydrocarbon ratios.

Table 3. Monthly mean OH and HO_2 concentrations inferred from scaled calculated solar actinic flux as described in the text.

Month	OH/10^5 cm^{-3}	HO_2/10^7 cm^{-3}
January	4.6	2.0
February	3.0	1.4
March	1.7	0.78
April	1.1	0.26
May	(1.0)	0.03
June	(1.0)	0
July	(1.0)	0
August	1.1	0.15
September	1.6	0.70
October	3.6	1.6
November	4.6	1.9
December	5.1	2.1

9 Conclusions

OH and HO_2 radicals were measured at Halley, Antarctica during January and February 2005, with mean radical levels of 3.9×10^5 molecule cm^{-3} for OH, and 0.76 ppt for HO_2. Typical maximum (local noontime) levels were 7.9×10^5 molecule cm^{-3} and 1.50 ppt respectively. These levels are consistent with earlier measurements of OH on the Antarctic Peninsula, but lower than recent observations from South Pole and Summit, Greenland. The main sources of HO_x were photolysis of O_3 and HCHO, with potentially important but uncertain contributions from HONO and higher aldehydes.

Of the measured OH sinks, reaction with CO and CH_4 dominated, giving a total OH lifetime of approximately 2 seconds; however the observed OH levels together with calculated HO_2 to OH conversion fluxes indicated that additional co-reactants were likely to have been present.

Elevated levels of NO_x resulting from snowpack photochemistry contributed to HO_x cycling and enhanced levels of OH, however the halogen oxides IO and BrO dominated the CH_3O_2 – HO_2 – OH conversion in this environment, with associated ozone destruction. The quantitative impact of this chemistry depends upon the details of the XO + CH_3O_2 reactions and magnitude of the aerosol sink for HOX, which are poorly constrained. HONO levels of several ppt were measured during CHABLIS, indicating a substantial additional HO_x and NO_x source, which we are currently unable to reconcile with the radical observations. Considering the enhanced HO_2 to OH conversion in the presence of the halogen species, the observed OH levels indicate that substantial unmeasured OH sinks are present. Data from the Arctic suggest that these may be higher oxygenated VOCs such as acetaldehyde, although the halogen halides HI and HBr are alternative candidates.

The fast photochemistry and hence oxidising environment of the boundary layer in coastal Antarctica is a complex regime affected by NO_x, VOC and halogen chemistry, rather than a quiescent regime of low HO_x production through ozone photolysis coupled with straightforward removal through reaction with CO and CH_4. This being the case, extrapolating from the local atmospheric chemical environment, as might be determined from analyses of air from firn and ice cores collected in polar regions, to the prevailing free tropospheric chemical composition may be difficult.

Acknowledgements. We wish to thank Z. Fleming, G. Mills, K. Read and A. Saiz-Lopez for their help and contributions to the CHABLIS project, in Antarctica and beyond. The logistic assistance and support from the staff of the British Antarctic Survey is also gratefully acknowledged. We also thank T. Ingham, C. Floquet and S. Smith in Leeds, who allowed us the use of their equipment in support of the campaign. CHABLIS was funded by the Natural Environment Research Council through the Antarctic Funding Initiative, ref. NER/G/S/2001/00558.

Edited by: W. T. Sturges

References

Anderson, P. S.: Behaviour of tracer diffusion in simple atmospheric boundary layer models, Atmos. Chem. Phys. Discuss. 6, 13 111–13 138, 2006.

Aschmutat, U., Hessling, M., Holland, F. and Hofzumahaus, A.: A tuneable source of hydroxyl (OH) and hydroperoxy (HO_2) radicals: In the range between 10^6 and 10^9 cm^{-3}, Physico-Chemical Behaviour of Atmospheric Pollutants, edited by: Angeletti, G. and Restelli, C., Proc. EUR 15609, 811–816, 1994.

Bauguitte, S. J.-B., Bloss, W. J., Clemitshaw, K. C., Evans, M. J., Jones, A. E., Lee, J. D., Mills, G., Saiz-Lopez, A., Salmon, R. A., Roscoe, H. K., and Wolff, E. W.: An overview of year-round NOx measurements during the CHABLIS campaign: can sources and sinks estimates unravel observed diurnal cycles?, Geophys. Res. Abstr., 8, 09054, 2006.

Berresheim, H., Plass-Dülmer, C., Elste, T., Mihalopoulos, N., and Rohrer, F.: OH in the coastal boundary layer of Crete during MINOS: Measurements and relationship with ozone photolysis, Atmos. Chem. Phys., 3, 639–649, 2003, http://www.atmos-chem-phys.net/3/639/2003/.

Bloss, W. J., Gravestock, T. J., Heard, D. E., Ingham, T., Johnson, G. P., and Lee, J. D.: Application of a compact all-solid-state laser system to the in situ detection of atmospheric OH, HO_2, NO and IO by laser-induced fluorescence, J. Environ. Monit. 5, 21–28, 2003.

Bloss, W. J., Lee, J. D., Johnson, G. P., Sommariva, R., Heard, D. E., Saiz-Lopez, A., Plane, J. M. C., McFiggans, G., Coe, H., Flynn, M., Williams, P., Rickard, A. R., and Fleming, Z. L.: Impact of halogen monoxide chemistry upon boundary layer OH and HO_2 concentrations at a coastal site, Geophys. Res. Lett., 32, L06814, doi:10.1029/2004GL022084, 2005a.

Bloss, W. J., Evans, M. J., Lee, J. D., Sommariva, R., Heard, D. E., and Pilling, M. J.: The oxidative capacity of the troposphere: Coupling of field measurements of OH and a global chemistry transport model, Faraday Discuss.,130, 425–436, 2005b.

Boudries, H., Bottenheim, J. W., Guimbaud, C., Grannas, A. M., Shepson, P. B., Houdier, S., Perrier, S., and Dominé, F.: Distribution and trends of oxygenated hydrocarbons in the high Arctic derived from measurements in the atmospheric boundary layer and interstitial snow air during the ALERT2000 field campaign, Atmos. Environ., 36, 2573–2583, 2002.

Brauers, T., Hausmann, M., Bister, A., Kraus, A., and Dorn, H. P.: OH radicals in the boundary layer of the Atlantic Ocean 1. Measurements by long-path laser absorption spectroscopy, J. Geophys. Res., 106, 7399–7414, 2001.

Cantrell, C. A., Zimmer, A., and Tyndall, G.S.: Absorption cross sections for water vapour from 183 to 193 nm, Geophys. Res. Lett., 24, 17, 2195–2198, 1997.

Chen, G., Davis, D., Crawford, J., Nowak, J.B., Eisele, F., Mauldin III, R.L., Tanner, D., Buhr, M., Shetter, R., Lefer, B., Arimoto, R., Hogan, A., and Blake, D.: An Investigation of South Pole HOx Chemistry: Comparison of Model Results with ISCAT Observations, Geophys. Res. Lett., 28, 3633–3636, 2001.

Chen, G., Davis, D., Crawford, J., Hutterli, L. M., Huey, L. G., Slusher, D., Mauldin, L., Eisele, F., Tanner, D., Dibb, J., Buhr, M., McConnell, J., Lefer, B., Shetter, R., Blake, D., Song, C. H., Lombardo, K., and Arnoldy, J.: A reassessment of HOx South Pole chemistry based on observations recorded during ISCAT 2000, Atmos. Environ., 38, 5451–5461, 2004.

Clemitshaw, K. C.: A Review of Instrumentation and Measurement Techniques for Ground-Based and Airborne Field Studies of Gas-Phase Tropospheric Chemistry, Critical Reviews in Environmental Science and Technology, 34, 1–108, 2004.

Clemitshaw, K. C.: Coupling between Tropospheric Photochemistry of Nitrous Acid (HONO) and Nitric Acid (HNO_3), Environ. Chem., 3, 31–34, 2006.

Creasey, D. J., Heard, D. E., and Lee, J. D.: Absorption cross-section measurements of water vapour and oxygen at 185 nm.

Implications for the calibration of field instruments to measure OH, HO_2 and RO_2 radicals, Geophys. Res. Lett. 27(11), 1651–1654, 2000

Creasey, D. J., Evans, G. E., Heard, D. E., and Lee, J. D.: Measurements of OH and HO_2 concentrations in the Southern Ocean marine boundary layer, J. Geophys. Res. 108, 4475, doi:10.1029/2002JD003206, 2003.

Davis, D., Nowak. J. B., Chen, G., Buhr, M., Arimoto, R., Hogan, A., Eisele, F., Mauldin, L., Tanner, D., Shetter, R., Lefer, B., and McMurry, P.: Unexpected High Levels of NO Observed at South Pole, Geophys. Res. Lett., 28, 3625–3628, 2001.

Davis, D., Chen, G., Buhr, M., Crawford, J., Lenschow, D., Lefer, B., Shetter, R., Eisele, F., Mauldin, L., and Hogan, A.: South Pole NOx Chemistry: an assessment of factors controlling variability and absolute levels, Atmos. Environ., 38, 5375–5388, 2004.

Davison, B., Hewitt, C. N., O'Dowd, C., Lowe, J. A., Smith, M. H., Schwikowski, M., Baltensperger, U. and Harrison, R. M., Dimetyl sulphide, methane sulphonic acid and the physiochemical aerosol properties in Atlantic air from the United Kingdom to Halley Bay, J. Geophys. Res. 101, 22 855–22 867, 1996.

Dibb, J. E., Huey, L. G., Slusher, D. L., and Tanner, D. J.: Soluble reactive nitrogen oxides at South Pole during ISCAT 2000, Atmos. Environ., 38, 5399–5409, 2004.

Dubey, M. K., Hanisco, T. F., Wennberg, P. O., and Anderson, J. G.: Monitoring potential photochemical interference in laser-induced fluorescence measurements of atmospheric OH, Geophys. Res. Lett., 23, 3215–3218, 1996.

Ehhalt, D. H. and Rohrer, F.: Dependence of the OH concentration on solar UV, J. Geophys. Res. 105, 3565–3571, 2000.

Grannas, A., M., Shepson, P. B., Guimbaud, C., Sumner, A. L., Albert, M., Simpson, W., Domine, F., Boudries, H., Bottenheim, J., Beine, H. J., Honrath, R., and Zhou, X.: A study of photochemical and physical processes affecting carbonyl compounds in the Arctic atmospheric boundary layer, Atmos. Environ., 36, 2733–2742, 2002.

Grannas, A. M., Shepson, P. B., and Filley, T. R.: Photochemistry and nature of organic matter in Arctic and Antarctic snow, Glob. Biogeochem. Cycles, 18, GB1006, doi:10.1029/2003GB002133, 2004.

Guimbaud, C., Grannas, A. M., Shepson, P. B., Fuentes, J. D., Boudries, H., Bottenheim, J. W., Dominé, F., Houdier, S., Perrier, S., Biesenthal, T. B. and Splawn, B. G.: Snowpack processing of acetaldehyde and acetone in the Arctic atmospheric boundary layer, Atmos. Environ., 36, 2743–2752, 2002.

Hard, T. M., O'Brien, R. J., Chan, Y. C., and Mehrabzadeh, A. A.: Tropospheric Free Radical Determination by FAGE, Environ. Sci. Tech., 18, 768–777, 1984.

Heard, D. E. and Pilling, M. J.: Measurement of OH and HO2 in the Troposphere, Chem. Rev. 103, 5163–5198, 2003.

Honrath, R. E., Peterson, M. C., Guo, S., Dibb, J. E., Shepson, P. B., and Campbell, B.: Evidence of NOx production within or upon ice particles in the Greenland snowpack, Geophys. Res. Lett., 26, 695–698, 1999.

Hofzumahaus, A., Aschmutat, U., Heßling, M., Holland, F., and Ehhalt, D. H.: The measurement of tropospheric OH radicals by laser-induced fluorescence spectroscopy during the POPCORN field campaign, Geophys. Res. Lett., 23, 2541–2544, 1996.

Holland, F., Hofzumahaus, A., Schäfer, R., Kraus, A., and Pätz, H. W.: Measurements of OH and HO2 radical concentrations and photolysis frequencies during BERLIOZ, J. Goephys. Res., 108(D4), 8246, doi:10.1029/2001JD001393, 2003.

Huey, L. G., Sjostedt, S., Tanner, D. J., Dibb, J., Chen, G., Lefer, B., Peischl, J., Hutterli, M., Blake, N., Blake, D., Beyersdorf, A., and Ryerson, T.: Measurements of OH and HO_2 + RO_2 at Summit Greenland, Eos Trans. AGU, 85(47), Fall Meet. Suppl., Abstract A22C-02, 2004.

Hutterli, M. A., Röthlisberger, R., and Bales, R. C.: Atmosphere-to-snow-to-firn transfer studies of HCHO at Summit, Greenland, Geophys. Res. Lett., 26, 1691–1694, 1999.

Jacob, D. J., Field, B. D., Li, Q., Blake, D. R., de Gouw, J., Warneke, C., Hansel, A., Wisthaler, A., Singh, H. B., and Guenther, A.: Global budget of methanol: Constraints from atmospheric observations, J. Geophys. Res., 100, D08303, doi:10.1029/2004JD005172, 2005.

Jefferson, A., Tanner, D. J., Eisele, F. L., Davis, D. D., Chen, G., Crawford, J., Huey, J. W., Torres, A. L., and Berresheim, H.: OH Photochemistry and methane sulphonic acid formation in the coastal Antarctic boundary layer, J. Geophys. Res., 103, 1647–1656, 1998.

Jones, A. E., Weller, R., Wolff, E. W., and Jacobi, H.-W.: Speciation and Rate of Photochemical NO and NO_2 Production in Antarctic Snow, Geophys. Res. Lett., 27, 345–348, 2000.

Kanaya, Y., Sadanaga, Y., Nakumura, K., and Akimoto, H.: Behavior of OH and HO_2 radicals during the Observations at a Remote Island of Okinawa (ORION99) field campaign: 1. Observation using a laser-induced fluorescence instrument, J. Geophys. Res., 106, 24 197–24 208, 2001.

Legrand, M. and Mayewski, P.: Glaciochemistry of Polar Ice Cores: A Review, Rev. Geophys. 35, 219–243, 1997.

Lewis, A. C., Hopkins, J. R., Carpenter, L. J., Stanton, J., Read, K. A., and Pilling, M. J.: Sources and sinks of acetone, methanol and acetaldehyde in North Atlantic marine air, Atmos. Chem. Phys., 5, 1963–1974, 2005, http://www.atmos-chem-phys.net/5/1963/2005/.

Liao, W., Case, A. T., Mastromarino, J., Tan, D., and Dibb, J. E.: Observations of HONO by laser-induced fluorescence at the South Pole during ANTCI 2003, Geophys. Res. Lett., 33, L09810, doi:10.1029/2005GL025470, 2006.

Madronich, S. and Flocke, S.: The role of solar radiation in atmospheric chemistry, in Handbook of Environmental Chemistry (P. Boule, Ed.), Springer Verlag, Heidelberg, 1–26, 1998.

Mauldin III, R. L., Eisele, F. L., Tanner, D. J., Kosciuch, E., Shetter, R., Lefer, B., Hall, S. R., Nowak, J. B., Buhr, M., Chen, G., Wang, P., and David, D.: Measurements of OH, H_2SO_4, and MSA at the South Pole during ISCAT, Geophys. Res. Lett., 28, 3629–3632, 2001.

Mauldin III, R. L., Tanner, D., Buhr, M., Shetter, R., Lefer, B., Arimoto, R., Hogan, A. and Blake, D.: An Investigation of South Pole HOx Chemistry: Comparison of Model Results with ISCAT Observations, Geophys. Res. Lett., 28, 3633–3636, 2001.

Mauldin III, R. L., Kosciuch, E., Henry, B., Eisele, F. L., Shetter, R., Lefer, B., Chen, G., Davis, D., Huey, G., and Tanner, D.: Measurements of OH, HO_2+RO_2, H_2SO_4 and MSA at the South Pole during ISCAT 2000, Atmos. Environ., 38, 5423–5437, 2004.

Penkett, S. A., Monks, P. S., Carpenter, L. J., and Clemitshaw, K. C.: Relationships between ozone photolysis rates and peroxy radical concentrations in clean marine air over the Southern

Ocean, J. Geophys. Res., 102, 12 805–12 817, 1997.

Read, K. A., Lewis, A. C., Salmon, R. A., Jones, A. E., and Bauguitte, S.: OH and halogen atom influence on the variability of non-methane hydrocarbons in the Antarctic Boundary Layer, Tellus B, 59, 22–38, 2007.

Rohrer, F. and Berresheim, H.: Strong correlation between levels of tropospheric hydroxyl radicals and solar ultraviolet radiation, Nature, 442, 184–187, 2006.

Saiz-Lopez, A., Mahajan, A. S., Salmon, R. A., Bauguitte, S. J.-B., Jones, A. E., Roscoe, H. K. and Plane, J. M. C, Boundary layer halogens in coastal Antarctica, Science, 317, 348–351, 2007a.

Saiz-Lopez, A., Plane, J. M. C., Mahajan, A. S., Anderson, P. S., Bauguitte, S. J.-B., Jones, A. E., Salmon, R. A., Bloss, W. J., Lee, J. D., and Heard, D. E.: On the vertical distribution of boundary layer halogens over coastal Antarctica: implications for O_3, HO_x, NO_x and the Hg lifetime, Atmos. Chem. Phys. Discuss. 7, 9385–9417, 2007b.

Sander, S. P., Friedl, R. R., Golden, D. M., Kurylo, M. J., Moortgat, G. K., Keller-Rudek, H., Wine, P. H., Ravishankara, A. R., Kolb, C. E., Molina, M. J., Finlayson-Pitts, B. J., Huie, R. E., and Orkin, V. L.: Chemical Kinetics and Photochemical Data for Use in Atmospheric Studies - Evaluation Number 15, NASA-JPL Publication 06-2, Jet Propulsion Laboratory, California Institute of Technology, Pasadena, CA, 2006.

Sjostedt, S. J., Huey, L. G., Tanner, D. J., Peischl, J., Chen, G., Dibb, J. E., Lefer, B., Hutterli, M. A., Beyersdorf, A. J., Blake, N. J., Blake, D. R.: Peroxy and Hydroxyl Radical Measurements During the Spring 2004 Summit Field Campaign, Eos Trans. AGU, 86(52), Fall Meet. Suppl., Abstract A24A-02, 2005.

Smith, S. C., Lee, J. D., Bloss, W. J., Johnson, G. P., Ingham, T., and Heard, D. E.: Concentrations of OH and HO_2 radicals during NAMBLEX: Measurements and steady state analysis, Atmos. Chem. Phys., 6, 1435–1453, 2006, http://www.atmos-chem-phys.net/6/1435/2006/.

Sumner, A.-L. and Shepson, P. B.: Snowpack production of formaldehyde and its effect on the Arctic troposphere, Nature, 398, 230–233, 1999.

Tan. D., Faloona, I., Simpas, J. B., Brune, W., Olson, J., Crawford, J., Avery, M., Sachse, G., Vay, S., Sandholm, S., Guan, H.-W., Vaughn, T., Mastromarino, J., Heikes, B., Snow, J., Podolske, J., and Singh, H.: OH and HO_2 in the tropical Pacific: Results from PEM-Tropics B, J. Geophys. Res., 106, 32 667–32 681, 2001.

Walker, S. J., Jackson, A. V., Evans, M. J., McQuaid, J. B., and Salmon, R.: Assessment of hydrogen peroxide in the coastal Antarctic boundary layer, Geophys. Res. Abstr., 8, 03740, 2006.

Washida, N., Mori, Y., and I. Tanaka: Quantum Yield of Ozone Formation from Photolysis of the Oxygen molecule at 1849 and 1931 Å, J. Chem. Phys., 54, 1119–1122, 1971.

Zhou, X., Beine, H., Honrath, R. E., Fuentes, J. D., Simpson, W., Shepson, P. B., and Bottenheim, J. W.: Snowpack Photochemical Production of HONO: a Major source of OH in the Arctic Boundary Layer in Springtime, Geophys. Res. Lett., 28, 4087–4090, 2001.